AIAA JOURNAL
Vol. 47, No. 7, July 2009

Acoustic Damping of a Helmholtz Resonator with an Oscillating Volume

D. Zhao*
University of Cambridge, Cambridge, England CB2 1PZ, United Kingdom
C. A'Barrow†
Loughborough University, Leicestershire, England LE11 3TU, United Kingdom
A. S. Morgans‡
Imperial College London, London, England SW7 2AZ, United Kingdom
and
J. Carrotte§
Loughborough University, Leicestershire, England LE11 3TU, United Kingdom

DOI: 10.2514/1.39704

Combustion instabilities are caused by a coupling between acoustic waves and unsteady heat release. Helmholtz resonators are widely used as acoustic dampers to stabilize unstable combustion systems. Such dampers are typically subjected to a low Mach number grazing flow and are normally only effective over a narrow frequency range, close to the resonant frequency. To increase the effective frequency range, a Helmholtz resonator with an oscillating volume, implemented via an electromagnetic shaker and vibrating backplate, was designed and experimentally tested at the University of Loughborough. It was found that volume oscillation can either increase or decrease the acoustic power being absorbed by the resonator, depending on the phase with which it is driven. A nonlinear numerical model of a Helmholtz resonator with an oscillating volume was then developed to simulate the experiments. Excellent agreement between the numerical and experimental results is found. Furthermore, insight into how to obtain maximum power absorption was provided by the numerical model and validated by the experiments. Finally, to optimize the phase in real time (by minimizing the amplitude of the pressure oscillations), active control of the backplate vibration was experimentally investigated. For the low Mach number grazing-flow regime investigated, this was found to give increased damping and to increase the effective frequency range of the resonator.

Nomenclature

c	=	speed of sound, m/s
K	=	discharge coefficient
k	=	pressure transducers
L_i	=	left propagating waves
M	=	Mach number
p	=	pressure, Pa
R_d	=	downstream reflection coefficient
R_i	=	right propagating waves
R_u	=	upstream reflection coefficient
S	=	cross-sectional area, m^2
t	=	time, s
u	=	velocity, m/s
V	=	cavity volume, m^3
$\dot{V}$	=	volume flow rate, m^3/s
x	=	axial position
$\mathbf{X}$, $\mathbf{Y}$	=	coefficient matrix
Δ	=	power absorption coefficient
Δt	=	time steps, s
κ	=	end correction coefficient
ρ	=	density, kg/m^3
ϕ	=	phase difference between the pressure perturbations across the resonator neck, deg;
ψ	=	phase difference between the backplate acceleration and the neck pressure perturbation, deg
ω	=	radian frequency, rad/s

Subscripts

ca	=	resonator cavity
d	=	downstream open end
eff	=	effective length
h	=	Helmholtz resonator neck position
i	=	variable zones
ls	=	loudspeakers
opt	=	optimum phases
p	=	pipe
tot	=	total length
u	=	upstream open end

Presented as Paper 2804 at the 14th AIAA/CEAS Aeroacoustics Conference, Vancouver, British Columbia, Canada, 5–7 May 2008; received 14 July 2008; revision received 31 March 2009; accepted for publication 8 March 2009.

*Ph.D. Student, Engineering Department. Member AIAA.
†Ph.D. Student, Department of Aeronautical and Automotive Engineering.
‡Lecturer, Department of Aeronautics, Member AIAA.
§Reader, Department of Aeronautical and Automotive Engineering.

I. Introduction

SELF-EXCITED combustion oscillations are generated by the interaction between acoustic waves and combustion. Unsteady heat release generates acoustic waves; these propagate within the combustor and reflect from boundaries to arrive back at the combustion zone, in which they cause more unsteady heat release. Under certain conditions, this feedback can result in large and damaging self-excited oscillations.

Helmholtz resonators (HRs) are widely used in combustion systems as acoustic dampers to stabilize combustion instabilities [1]. At resonance, a large volume of fluid in the cavity compresses and expands periodically, as the mass of fluid in the neck vibrates. The damping mechanism is primarily due to thermoviscous and vortex-shedding losses [2–5]. The resonant frequency of HRs is given approximately by $\omega^2 = c^2 S/Vl_{\text{eff}}$, where S and l_{eff} are the neck

cross-sectional area and effective length, respectively; V is the volume of the resonator cavity; and c is the speed of sound [6]. If the frequency of the unstable mode in the combustion system is close to the HR resonant frequency, the HR can efficiently dissipate acoustic energy. However, the effective frequency range of HRs is normally narrow and lower frequencies require physically large dampers, which can be difficult to implement within an engine environment.

There is currently interest in approaches that are able to increase the effective frequency range of Helmholtz resonators. One such approach is tuned passive control, which exploits the fact that the resonant frequency can be varied by altering the resonator geometry [7–12]: for example, by changing the neck area. An alternative approach, which is the one being investigated in this paper, is to oscillate the resonator volume [13–18]. This could be more attractive than, say, changing the neck area (which potentially requires 2 components to slide relative to one another) in what is a hostile environment, although there are still clearly practical issues to be overcome for such a device to be successfully used. However, it will be shown later that if practically feasible, oscillation of the cavity volume can either increase or decrease the viscous effects of the movement of the neck flow and hence the acoustic power being absorbed.

In this paper, investigations into the effect of volume oscillation consist of both modeling and experiments. A Helmholtz resonator with an oscillating volume was experimentally investigated in a pipe system at the University of Loughborough. This is described in Sec. II. The backplate was driven via an electromagnetic shaker and a signal generator, for which the phase could be varied. In Sec. III, a model for the damping effect of a HR with an oscillating volume is developed. A nonlinear HR model is coupled with the linearized flow-conservation equations along the pipe. In Sec. IV, the numerical and experimental results are compared and discussed. In Sec. V, using the numerical and experimental results, design guidance rules for optimizing the damping performance of a Helmholtz resonator with an oscillating volume are extracted. Finally, in Sec. VI, we experimentally demonstrate that active control of a HR volume oscillation can greatly increase its damping over a broad frequency range.

II. Description of the Experiment

To investigate the effect of volume oscillation on acoustic damping, a Helmholtz resonator with an oscillating volume was experimentally investigated. The experimental setup is shown in Fig. 1. A Helmholtz resonator with a vibrating backplate was connected to an open-ended pipe with a circular cross section of 120 mm diameter (corresponding to a cuton frequency of approximately 1700 Hz). This ensured that all nonplanar modes were well cut off for the frequency range of interest. The total length of the pipe, x_{tot_p}, was 4.03 m. Attached to this pipe were two loudspeakers for acoustic excitation at the same axial length.

The HR backplate consisted of an aluminum plate attached to an electromagnetic shaker. A seal was provided by a rubber diaphragm that was attached both to the aluminum plate and the rigid sidewalls of the resonator cavity. In combustion-related applications, the resonator neck may be subject to a very-low Mach number grazing flow [19]. Hence, a centrifugal fan was used to draw a small amount of flow along the pipe and past the resonator neck with a velocity of order 1 m/s. Five pressure transducers ($k1$, $k2$, $k3$, $k4$, and $k5$) were used to measure the pressure perturbations along the pipe (at −1.83, −2.27, −2.45, −2.67, and −2.81 m, respectively). These were spaced to maximize the accuracy of the mode shape definitions within the pipe over the frequency range of interest. One pressure transducer, $k6$, was located inside the resonator cavity. An accelerometer was attached to the resonator backplate to measure its acceleration. A LabVIEW program was developed to generate driving signals to the backplate and the loudspeakers. The backplate and loudspeakers were always driven at the same frequency, but the phase difference between them could be varied.

The geometry of the experimental setup and the HR are summarized in Table 1. An overbar denotes a mean value.

III. Description of the Numerical Model

An axial pipe system with both ends open is simulated, corresponding to the experimental setup at the University of Loughborough, as shown in Fig. 2. In the experiments, loudspeakers were used as sound sources to generate the plane waves propagating along the pipe. In the numerical model, these are simulated as point monopoles. A signal simulator is applied to generate phase-shifted signals to control the backplate velocity and the loudspeakers' volume flow rate.

The mean flow is assumed to be steady and one-dimensional. The flow fluctuations are modeled as being due to plane acoustic waves traveling in opposite directions. The wave strengths are denoted by $R_1(t)$, $L_1(t)$, $R_2(t)$, $L_2(t)$, $R_3(t)$, and $L_3(t)$ in different regions, as shown in Fig. 2. Contributions from vorticity and entropy waves are neglected, and the acoustic waves are assumed to behave linearly with respect to the mean flow. If we let L_i denote the acoustic wave strengths of $L_1(t)$, $L_2(t)$, or $L_3(t)$ and R_i denote $R_1(t)$, $R_2(t)$, or $R_3(t)$, the equations for the pressure fluctuations are given by

$$p'(x,t) = R_i\left(t - \frac{x}{\bar{c}+\bar{u}}\right) + L_i\left(t + \frac{x}{\bar{c}-\bar{u}}\right) \tag{1a}$$

$$u'(x,t) = \frac{1}{\bar{\rho}\,\bar{c}}\left[R_i\left(t - \frac{x}{\bar{c}+\bar{u}}\right) - L_i\left(t + \frac{x}{\bar{c}-\bar{u}}\right)\right] \tag{1b}$$

$$\rho'(x,t) = \frac{1}{\bar{c}^2}\left[R_i\left(t - \frac{x}{\bar{c}+\bar{u}}\right) + L_i\left(t + \frac{x}{\bar{c}-\bar{u}}\right)\right] \tag{1c}$$

where p denotes the pressure, u is the flow velocity, ρ is the density, and c speed of sound. A prime denotes a perturbation.

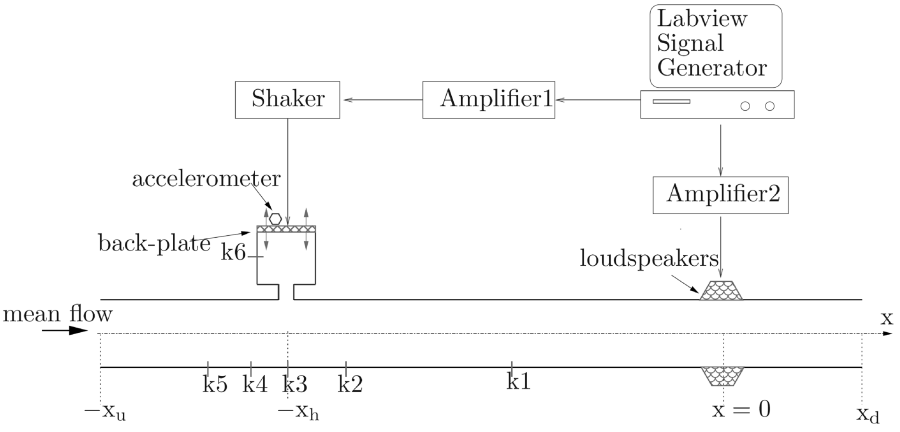

Fig. 1 Schematic of the experimental setup.

Table 1 Geometry of the experimental pipe system

Parameter	Value
Axial distance from the HR to loudspeakers, x_h, m	2.48–2.65
Axial distance from the upstream end to loudspeakers, x_u, m	3.78–3.95
HR cavity volume $\bar{V}$, m^3	$4.1–4.25 \times 10^{-4}$
Pipe cross-sectional area, S_p, m^2	1.13×10^{-2}
Cross-sectional area of the HR neck, S, m^2	2.35×10^{-4}

The pipe boundaries are modeled using pressure reflection coefficients R_u at the upstream open end and R_d at the downstream open end. The acoustic wave strengths on either side of the resonator are related by combining the flow-conservation equations. A nonlinear model of a Helmholtz resonator with an oscillating volume is used, which is an extension of the nonlinear discharge coefficient model used in several previous studies [2,3,5].

Momentum balance and mass continuity across the resonator neck give

$$(\partial/\partial t)\begin{pmatrix} u'_h(t) \\ p'_{ca}(t) \end{pmatrix} = \begin{pmatrix} -|u'_h(t)|K/l_{eff} & -1/\bar{\rho} l_{eff} \\ \bar{\rho}\bar{c}^2 S/\bar{V} & 0 \end{pmatrix}\begin{pmatrix} u'_h(t) \\ p'_{ca}(t) \end{pmatrix} + \begin{pmatrix} p'_h(t)/\bar{\rho} l_{eff} \\ (-\bar{\rho}\bar{c}^2/\bar{V})(\partial V'(t)/\partial t) \end{pmatrix} \quad (2)$$

where K is the discharge coefficient, $u'_h(t)$ is the flow velocity through the resonator neck, $p'_{ca}(t)$ is the cavity pressure of the resonator, and l_{eff} is the neck effective length.

Compared with the nonlinear HR model [2,3,5,20], Eq. (2) for a Helmholtz resonator with an oscillating volume includes an additional $(-\bar{\rho}\bar{c}^2/\bar{V})(\partial V'/\partial t)$ term. This captures the fact that the rate of mass change in the resonator cavity is now affected by both density and volume changes.

The loudspeakers are assumed to be sufficiently short compared with the acoustic wave length that they can be modeled as point monopoles located at $x = 0$. The acoustic wave strengths on either side of the loudspeakers are related by applying the linearized flow-conservation equations across the loudspeakers. Thus, the pipe end boundary conditions, the flow-conservation equations across the resonator and the loudspeakers, and the nonlinear model of a Helmholtz resonator with an oscillating volume provide enough information to solve for each of the six wave strengths in Fig. 2. The resulting matrix equation is given by

$$\mathbf{X}\cdot\begin{pmatrix} L_1(t) \\ R_2(t) \\ L_2(t) \\ R_3(t) \end{pmatrix} = \mathbf{Y}\cdot\begin{pmatrix} L_1\left(t-\frac{2(x_u-x_h)}{\bar{c}(1-\bar{M}^2)}\right) \\ R_2\left(t-\frac{x_h}{(\bar{c}+\bar{u})}\right) \\ L_2\left(t-\frac{x_h}{(\bar{c}-\bar{u})}\right) \\ R_3\left(t-\frac{2x_d}{\bar{c}(1-\bar{M}^2)}\right) \end{pmatrix} + \begin{pmatrix} \frac{-\bar{\rho}\bar{c}u'_h(t)S}{2S_p} \\ \frac{-\bar{\rho}\bar{c}u'_h(t)S}{2S_p} \\ 0 \\ \frac{\bar{\rho}\bar{c}\dot{V}_{ls}}{S_p} \end{pmatrix} \quad (3)$$

where $\bar{M}$ is the mean Mach number, $\dot{V}_{ls}$ is the volume flow rate of the loudspeakers, and $\mathbf{X}$ and $\mathbf{Y}$ are coefficient matrices, shown in the Appendix.

The power absorption coefficient, which denotes the fraction of incident energy being absorbed, is defined as a function of the wave strengths of $R_1(t)$, $L_2(t)$, $L_1(t)$, and $R_2(t)$ as

$$\Delta = 1 - \left(\frac{|R_1(t)|^2 + |L_2(t)|^2}{|L_1(t)|^2 + |R_2(t)|^2}\right)^{-1} \quad (4)$$

In the experiments, the two-microphone technique [21] was used to determine the wave strengths of $R_1(t)$, $L_2(t)$, $L_1(t)$, and $R_2(t)$ and hence the power absorption coefficient. In the numerical model, the wave strengths are determined numerically by solving the coupled equations (2) and (3).

IV. Comparison Between Numerical and Experimental Results

A. Choosing Parameters for the Numerical Model

Various parameters had to be chosen for the numerical model, as shown in Table 2. They were chosen to give a close match to the experimentally measured mode shape and power absorption curves for the Helmholtz resonator with a fixed volume (i.e., no volume oscillation). It can be seen that the length of the pipe simulated in the numerical model just slightly exceeds the actual pipe length of 4.03 m. This takes account of the end correction for the open end. Furthermore, the end reflection coefficient were taken to be identical at the upstream and downstream ends (justified due to the low speed of the grazing flow). Good fits were obtained with $R_u = R_d = -0.943$, which is slightly less (in magnitude) than the theoretical value of -1 for an open end. This means that the numerical model is capturing some of the acoustic energy loss that occur.

In the absence of volume oscillation, the Helmholtz resonator had a resonant frequency of 189 Hz. The acoustic power absorption coefficient and the pressure phase change across the resonator neck, ϕ, are shown as a function of frequency in Fig. 3. The sound pressure level in the pipe was maintained at approximately 135 dB. The agreement between numerical and experimental power absorption plots is excellent near the resonant frequency, where the maximum power absorption occurs. Note that in the absence of volume oscillation, the pressure phase change across the neck at maximum power absorption is approximately 90 deg.

The mode shape along the pipe at the resonant frequency is shown in Fig. 4. The experiment was set up such that the resonator is approximately located at the pressure antinode to give maximum

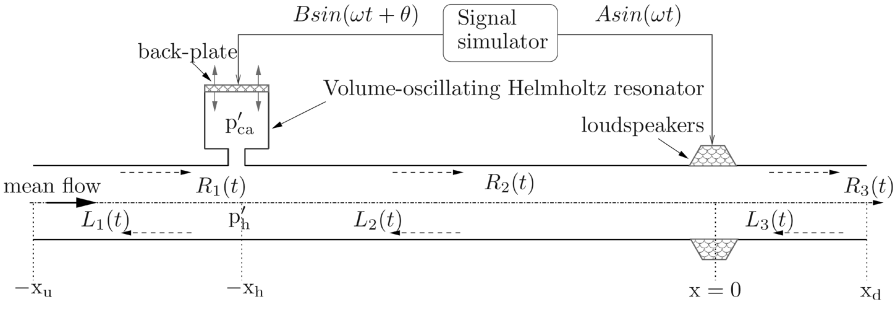

Fig. 2 Schematic of the numerical model.

Table 2 Parameters used in the numerical model

Parameter	Value
Axial distance from the HR to loudspeakers, x_h, m	2.45
Axial distance from the upstream end to loudspeakers, x_u, m	3.79
Effective length of the pipe, x_{tot}, m	4.07
HR cavity volume $\bar{V}$, m^3	4.2×10^{-4}
Reflection coefficients at upstream and downstream ends, R_u, R_d	−0.943
Discharge coefficient K	0.819
End correction coefficient for the pipe length, κ_1	1.32
End correction coefficient for the HR, κ_2	0.68
Time step Δt, s	1.0×10^{-4}

power absorption, and this is indicated by the mode shape along the pipe. There is excellent agreement between the numerical and the experimental mode shapes.

B. Results for the Helmholtz Resonator with an Oscillating Volume

We now investigate the damping effect of a Helmholtz resonator with an oscillating volume. The parameters presented in Table 2 were used in the numerical simulations; no additional tuning of any numerical parameters took place. The backplate vibration amplitude is denoted by the power settings of the shaker. With no backplate displacement, the pressure fluctuation recorded in the resonator cavity ($k6$) was measured with the loudspeakers activated (approximately 700 Pa). With the loudspeakers switched off, power to the shaker was applied and the cavity pressure fluctuations were measured. These were noted for different power settings and compared with those pressures generated by the loudspeaker forcing (and with no backplate vibration). A 100% shaker power denotes a pressure at $k6$ comparable with that generated by the loudspeakers (approximately 700 Pa), and 150% shaker power corresponds to approximately 1050 Pa.

With this 100% shaker power setting at frequencies of 150, 170, 184, and 210 Hz, the resonator damping effects are shown in Fig. 5. At each given frequency, the power absorption varies as the phase of the shaker signal varies, giving the vertical lines in Fig. 5. As already shown in Eq. (4), the power absorption coefficient has been normalized with respect to the incident wave energy. Thus, the maximum value cannot exceed +1.0, but the minimum value can be more negative than −1.0 (i.e., noise generation). However, this effect was not observed and so the scale is plotted from +1.0 to −1.0. The data clearly show that the oscillating volume can either increase or decrease the power absorbed, depending on the phase of the

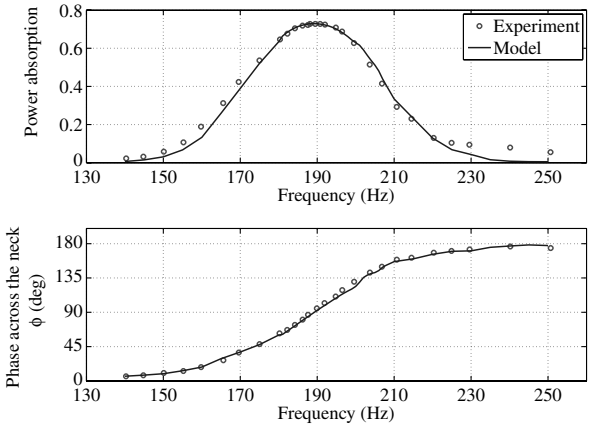

Fig. 3 Power absorption and phase across the neck characteristics of the Helmholtz resonator.

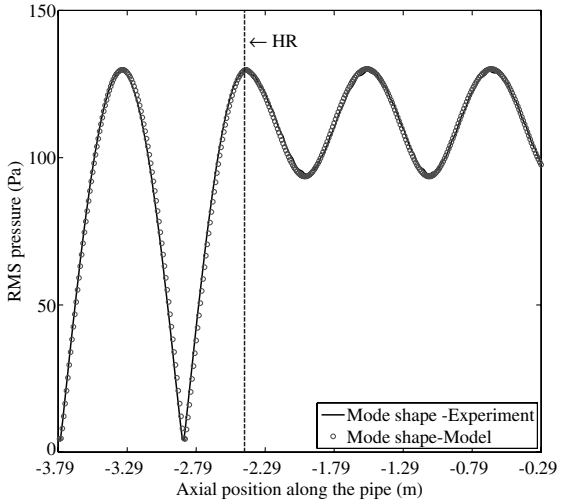

Fig. 4 RMS pressure fluctuations along the length of the test pipe at 189 Hz.

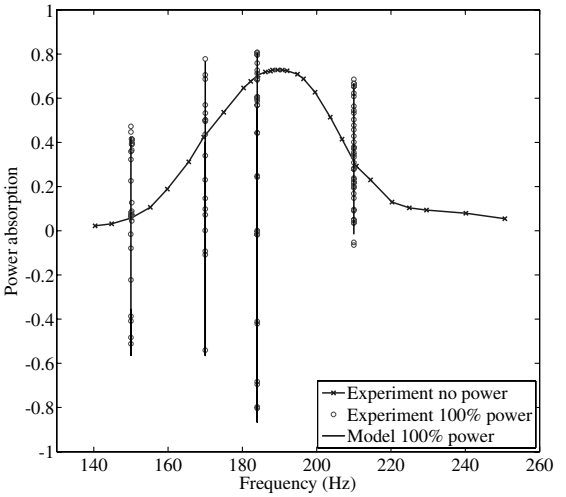

Fig. 5 Power absorption coefficient against the loudspeaker driving frequency.

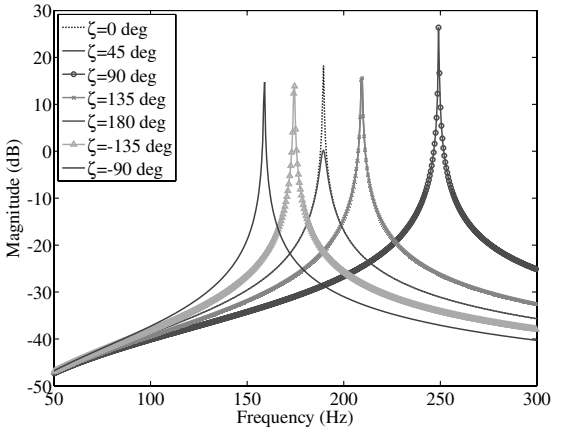

Fig. 6 Magnitude variations of the transfer function $\hat{u}_h(j\omega)/\hat{p}_h(j\omega)$ as the phase of the backplate forcing is varied.

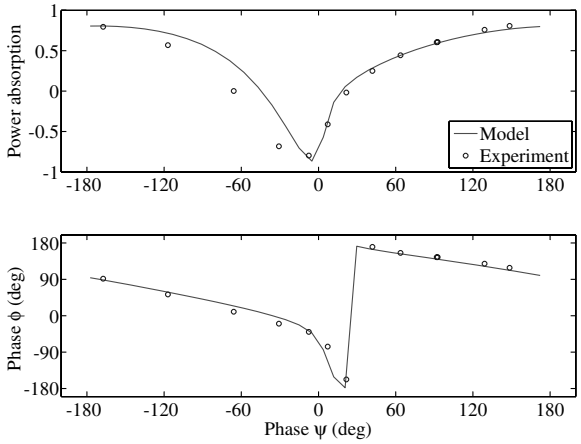

Fig. 7 Variations of power absorption and the phase ϕ with phase ψ at 184 Hz.

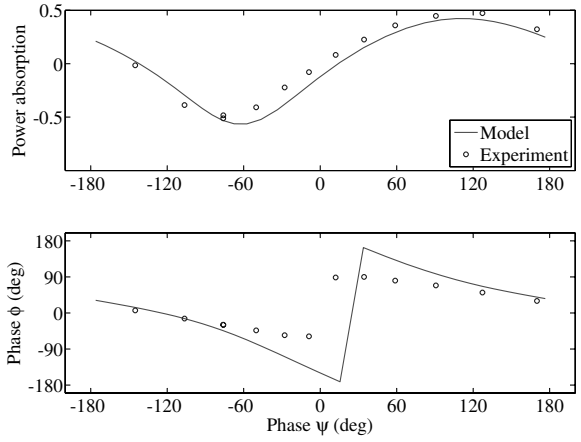

Fig. 8 Variations of power absorption coefficient and phase ϕ with phase ψ at 150 Hz.

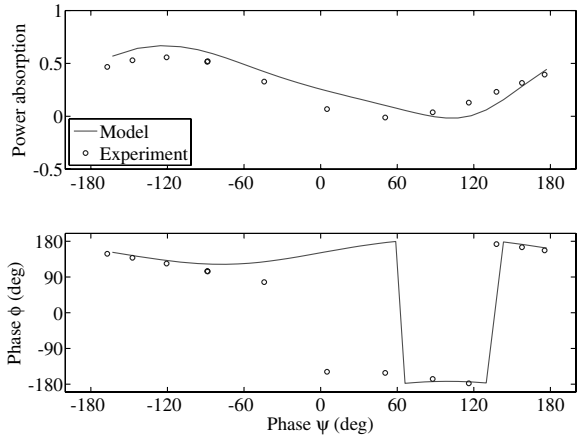

Fig. 9 Variations of power absorption coefficient and phase ϕ with phase ψ at 210 Hz.

oscillation. There is excellent agreement between the numerical and experimental results in the range of power absorptions seen at each frequency. We will now perform more detailed investigations into the effect of shaker phase on the damping behavior of a Helmholtz resonator with an oscillating volume.

C. Volume Oscillation Effects on Resonant Frequency

As the resonator cavity volume oscillates, the mass continuity across the resonator neck depends on both density and volume oscillations, as shown in Eq. (5):

$$\bar{\rho} S u_h'(t) = \frac{\bar{V}}{\bar{c}^2} \frac{\partial p_{\mathrm{ca}}'(t)}{\partial t} + \bar{\rho} \frac{\partial V'(t)}{\partial t} \tag{5}$$

where $V'(t)$ denotes the backplate displacement.

The results presented in Fig. 5 have shown that under certain phase conditions, the power absorption can be dramatically increased. This is most likely due to the fact that the resonant frequency is shifted as the backplate is vibrated. Taking Laplace transforms of Eqs. (2) and (5) with discharge coefficient K set to 0, a transfer function between the flow velocity through the neck and neck pressure perturbation, $\hat{u}_h(j\omega)/\hat{p}_h(j\omega)$, can be established by coupling with the transfer function $\hat{V}(j\omega)/\hat{u}_h(j\omega)$ as

$$\frac{\hat{u}_h(j\omega)}{\hat{p}_h(j\omega)} = \frac{1}{\bar{\rho}\bar{c}^2 S/\bar{V} j\omega + \bar{\rho} l_{\mathrm{eff}} j\omega - \bar{\rho}\bar{c}^2 \hat{V}(j\omega)/\bar{V}\hat{u}_h(j\omega)} \tag{6a}$$

$$\frac{\hat{V}(j\omega)}{\hat{u}_h(j\omega)} = \left|\frac{\hat{V}}{\hat{u}_h}\right| e^{j\zeta} \tag{6b}$$

where ζ denotes the phase difference between $\hat{V}(j\omega)$ and the neck flow velocity $\hat{u}_h(j\omega)$. Figure 6 shows the magnitude of the frequency response of a Helmholtz resonator with an oscillating volume as the phase angle is varied. It is clear that the backplate vibration can shift the resonant frequency, enabling a large power absorption over a broad frequency range.

V. Optimizing the Damping Performance of a Helmholtz Resonator with an Oscillating Volume

To gain insight into the conditions under which the optimum shaker phase angle occurs, a parametric study was carried out. This suggested that the phase angle ψ between the backplate acceleration $\mathrm{d}^2V'(t)/\mathrm{d}t^2$ and the neck pressure $k3$ could be useful for design guidance. Furthermore, because it was known that for a constant volume HR, peak power absorption occurs when the pressure phase change across the neck, ϕ, is approximately 90 deg, the variations of power absorption and phase ϕ with the phase ψ were studied for an oscillating volume. For these studies, three frequencies were considered: one close to the resonant frequency of the HR, one above and one below.

Close to the resonant frequency (i.e., at a frequency of 184 Hz), the results are shown in Fig. 7. For the numerical model, the power absorption coefficient is maximized when the pressure phase change across the neck ϕ is approximately 91 deg and when ψ is approximately 173 deg; for the experiments, these values were approximately $\phi \approx 92$ deg and $\psi \approx 192$ deg. Thus, the predicted and measured optimum phases are in close agreement.

Table 3 Comparison between the numerical optimum phases of ϕ and ψ and the experimental ones

Frequency, Hz	Experiment ϕ_{opt}, deg	Model ϕ_{opt}, deg	Experiment ψ_{opt}, deg	Model ψ_{opt}, deg
150	$\phi_{\mathrm{opt}} = 51.17 \pm 30$	$\phi_{\mathrm{opt}} = 74.25$	$\psi_{\mathrm{opt}} = 127.01 \pm 30$	$\psi_{\mathrm{opt}} = 117.2$
170	$\phi_{\mathrm{opt}} = 76.06 \pm 30$	$\phi_{\mathrm{opt}} = 71.81$	$\psi_{\mathrm{opt}} = 132.18 \pm 30$	$\psi_{\mathrm{opt}} = 148.2$
184	$\phi_{\mathrm{opt}} = 91.61 \pm 30$	$\phi_{\mathrm{opt}} = 90.85$	$\psi_{\mathrm{opt}} = 191.65 \pm 30$	$\psi_{\mathrm{opt}} = 172.87$
210	$\phi_{\mathrm{opt}} = 123.9 \pm 30$	$\phi_{\mathrm{opt}} = 133.67$	$\psi_{\mathrm{opt}} = 240.0 \pm 30$	$\psi_{\mathrm{opt}} = 234.6$

Table 4 Variation of optimum phase ϕ and ψ with acoustic frequency ω presented in the pipe

ω, rad/s	ϕ, deg	ψ, deg
$\omega > \omega_0$	$\phi_{opt} > 90$	$\psi_{opt} > 180$
$\omega < \omega_0$	$\phi_{opt} < 90$	$\psi_{opt} < 180$
$\omega = \omega_0$	$\phi_{opt} \approx 90$	$\psi_{opt} \approx 180$

The results below (150 Hz) and above (210 Hz) the resonant frequency of the HR are shown in Figs. 8 and 9 respectively. It can be seen that the matching between the experimental and numerical results is slightly less good than at the resonant frequency. This is likely to be because the numerical model parameters were optimized for behavior at the resonant frequency. However, qualitatively, the numerical and experimental results are in good agreement and revealed that below resonance, the optimum phase ϕ_{opt} is less than 90 deg and ψ_{opt} is less than 180 deg, whereas above resonance, ϕ_{opt} is greater than 90 deg and ψ_{opt} is greater than 180 deg. These findings are insightful for optimizing the resonator power absorption.

The numerical and experimental values of the optimum phases ϕ_{opt} and ψ_{opt} are summarized for four different frequencies in Table 3. The numerical and experimental results agree well and can be extrapolated to the more general rules summarized in Table 4, where ω_0 denotes the resonant frequency. This table provides guidance for the optimum design of a Helmholtz resonator with an oscillating volume.

VI. Active Control of a Helmholtz Resonator with an Oscillating Volume

So far, we have shown that vibrating the resonator backplate can either increase or decrease its damping performance. This depends on the phase of the backplate vibration. It is interesting now to experimentally investigate whether it is possible to use active control of the phase with which the volume is oscillated, to maximize the damping effect. A useful start point is to investigate minimizing the neck pressure amplitude $k3$ by active control of the backplate vibration.

The control approach is a two-stage control algorithm, which is to track and minimize in real time the pressure signal measured by the pressure transducer at the resonator neck ($k3$), as shown in Fig. 10. This measured pressure is fed to a real-time mode characterization algorithm [7], which analyzes the signal and provides the frequency and amplitude of the dominant mode. This information is passed to a two-stage control algorithm. The first stage identifies whether the frequency present in the system is below or above the resonant frequency of the HR and chooses an initial guess of the optimum backplate phase according to Table 4. Even though in our experiment the forcing frequency was known exactly, this would not be true for a general combustion system, and so the frequency was initially assumed to be unknown. The second stage uses the amplitude information to vary the backplate phase to minimize the pressure amplitude using a revised Newton–Raphson method. The amplitude of the backplate vibration, denoted as a shaker power setting, can be varied. However, in the experiments, the shaker power setting was chosen to be set to either 150 or 100%.

The mode characterization algorithm and the two-stage control algorithm were implemented in LabVIEW 8.0, with the data acquisition system consisting of a National Instruments PCI 6229 and a BNC 2090 connector. More details about these two algorithms are given by Zhao and Morgans [7].

The effect of implementing this experimentally with a shaker power setting of 150% at a frequency of 150 Hz is shown in Fig. 11. It

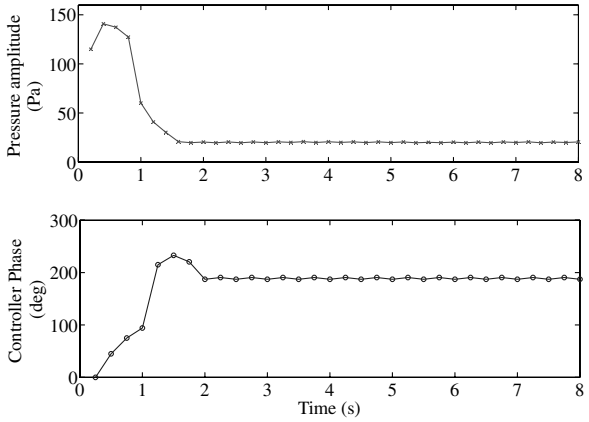

Fig. 11 Minimizing neck pressure amplitude by active control of the backplate vibration at 150 Hz, with a power setting of 150%.

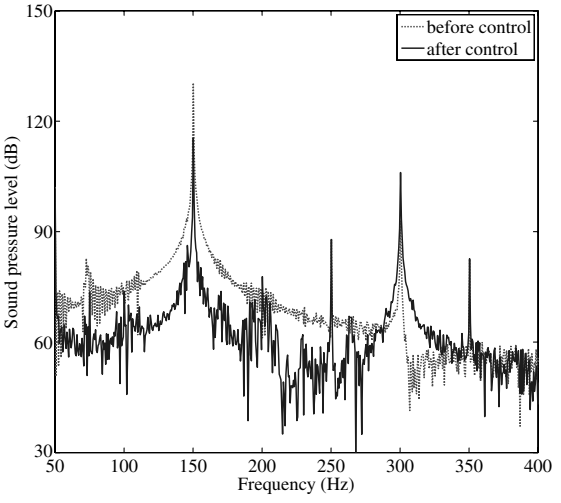

Fig. 12 Pressure spectra showing the damping effect of neck pressure by active control of backplate vibration at 150 Hz.

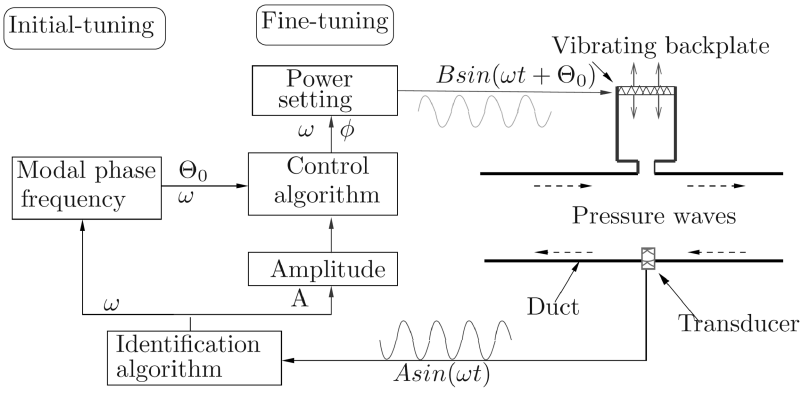

Fig. 10 Feedback control loop of active control.

is clear that once the backplate vibration is actively controlled, the neck pressure amplitude measured by $k3$ is significantly reduced from approximately 130 to 20 Pa. Correspondingly, the sound pressure level is reduced by approximately 16 dB, as shown in Fig. 12.

The effect of reducing the backplate power setting to 100% at the same frequency of 150 Hz is shown in Fig. 13. The amplitude of the measured pressure, $k3$, is reduced from 140 to approximately 105 Pa once the backplate vibration is actively controlled. The smaller reduction in the neck pressure amplitude is due to the reduced control authority of the lower backplate pressure setting.

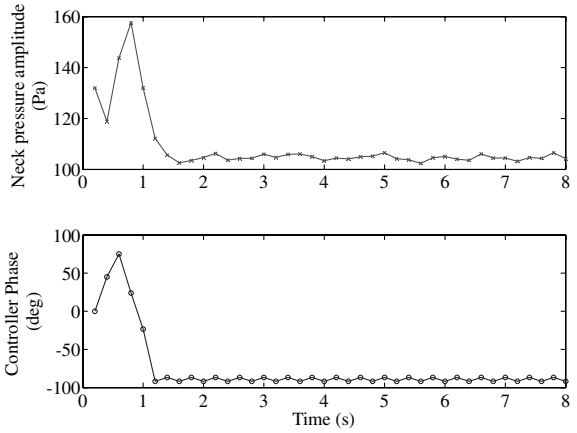

Fig. 13 Damping effect of active control at 150 Hz, with a backplate power setting of 100%.

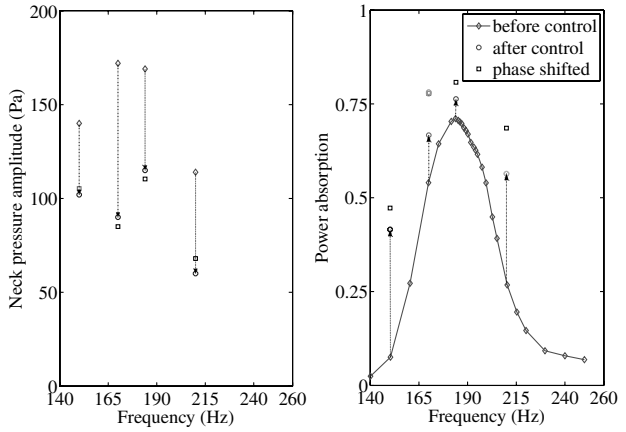

Fig. 14 Measured pressure amplitude reduction and the corresponding improvement of the power absorption due to backplate vibration with 100% power setting.

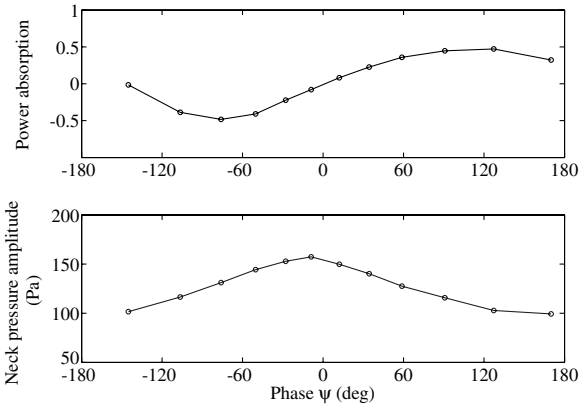

Fig. 15 Experimental variations of the power absorption coefficient and the neck pressure amplitude with the phase ψ at 150 Hz and a backplate power setting of 100%.

The results for frequencies of 170, 184, and 210 Hz are summarized in Fig. 14, with the shaker power of each individual frequency set to 100%. The effectiveness of active control is clearly demonstrated on both minimizing neck pressure amplitude and increasing power absorption (right graph). Note that for simplicity in this study, we have used active control to minimize a pressure amplitude at a specific location, rather than maximizing the acoustic power absorbed. These are clearly not the same thing (see Fig. 15), but for interest's sake, the effect of the active control on the power absorption at a backplate power setting of 100% is shown in Fig. 14 (right graph). The active control always increases the power absorption, although not to the maximum level achievable.

VII. Conclusions

Experiments showed that oscillating the volume of a Helmholtz resonator attached to a cold-flow pipe system can either increase or decrease the effectiveness of the Helmholtz resonator as a damping device. The frequency of the cavity volume oscillation was the same as that present acoustically in the system. The improvement or reduction in damping performance then depended on the phase of the volume oscillation for a given amplitude of backplate movement. Improvement was possible across a wide frequency range, making volume oscillation an ideal tool for widening the effective frequency range of a HR, as well as improving its damping performance.

A numerical model was developed to simulate the effect of the volume oscillation. The main additional effect to include was that of the cavity volume fluctuations on mass conservation through the HR neck. This alters the power absorption coefficient and means that the effective frequency range can be significantly broadened. The numerical model captured the main features of the experimental results very well.

To extract guidance for optimizing the performance of a Helmholtz resonator with an oscillating volume, numerical and experimental investigations were performed. General rules for choosing the phase of the volume oscillation relative to the pressure signal at the HR neck were obtained, with the experimental and numerical results being consistent with one another. These rules are insightful for optimizing the damping performance of a Helmholtz resonator with an oscillating volume.

Active control of the volume oscillation phase angle was performed experimentally. The frequency present in the system was identified and used to obtain a best guess of the optimum phase. The pressure oscillation amplitude at the HR neck was then minimized in real time, and it was found that this was very effective for optimizing the choice of phase angle.

The reported investigation was undertaken with the resonator being subjected to a low Mach number grazing flow, as typically found within a combustion system. However, it is thought that the principle could also be applied to higher Mach number grazing flows such as those found within various duct lining applications. However, this would require further work to be conducted at these higher grazing flows to confirm the potential benefits.

Appendix: Coefficient Matrices in the Resulting Matrix Equation

The full form of the coefficients in Eq. (3) is

$$\mathbf{X} = \begin{pmatrix} 0 & 1 & 0 & 0 \\ 1 & 0 & 0 & 0 \\ 0 & 0 & 1 & -1 \\ 0 & 0 & -1 & -1 \end{pmatrix} \qquad \mathbf{Y} = \begin{pmatrix} R_u & 0 & 0 & 0 \\ 0 & 0 & 1 & 0 \\ 0 & -1 & 0 & R_d \\ 0 & -1 & 0 & -R_d \end{pmatrix}$$

Acknowledgments

Dan Zhao's Ph.D. studentship is funded by Cambridge Overseas Trust, Cambridge University Board of Graduate Studies, and a Darwin College Scholarship. Chris A'Barrow is funded by Rolls-

Royce, plc. Aimee Morgans was supported as a Research Fellow by the Royal Academy of Engineering and the Engineering and Physical Sciences Research Council. Jon Carrotte was supported as a Reader in the University of Loughborough by Rolls-Royce, plc. This financial support is gratefully acknowledged. The authors thank Ann Dowling for her insights and suggestions and support and John Hazelwood for his technical support in this work.

References

[1] Richards, G. A., and Straub, D. L., "Passive Control of Combustion Instabilities in Stationary Gas Turbines," *Combustion Instabilities in Gas Turbine Engines*, edited by T. C. Lieuwen, and V. Yang, Vol. 210, AIAA, New York, 1985, pp. 533–575.

[2] Day, I. J., Dowling, A. P., Dupère, I. D. J., and Peyrache, C., "Acoustic Absorbers for LPP Combustors," Department of Engineering, Univ. of Cambridge, Cambridge, England, U.K., Feb. 2001.

[3] Zinn, B. T., "A Theoretical Study of Non-linear Damping by Helmholtz Resonators," *Journal of Sound and Vibration*, Vol. 13, No. 3, 1970, pp. 347–356. doi:10.1016/S0022-460X(70)80023-2

[4] Kinsler, L. E., Frey, A. R., Coppens, A. B., and Sanders, J. V., *Fundamentals of Acoustics*, Wiley, New York, 2000.

[5] Cummings, A., "Acoustic Nonlinearities and Power Losses at Orifices," *AIAA Journal*, Vol. 22, No. 6, 1984, pp. 786–792. doi:10.2514/3.8680

[6] Dowling, A. P., and Ffowcs-Williams, J., *Sound and Sources of Sound*, Halsted Press, Sydney, Australia, 1983.

[7] Zhao, D., and Morgans, A. S., "Tuned Passive Control of Combustion Instabilities using Multiple Helmholtz Resonators," *Journal of Sound and Vibration*, Vol. 320, No. 4, 2009, pp. 744–757. doi:10.1016/j.jsv.2008.09.006

[8] Wang, C. H., "Actively-Tuned Passive Control of Combustion Instabilities," Ph.D. Dissertation, Department of Engineering, Univ. of Cambridge, Cambridge, England, U.K., Apr. 2004.

[9] DeBedout, J. M., Franchek, M. A., Bernhard, R. J., and Mongeau, L., "Adaptive-Passive Noise Control with Self-Tuning Helmholtz Resonators," *Journal of Sound and Vibration*, Vol. 202, No. 1, 1997, pp. 109–123. doi:10.1006/jsvi.1996.0796

[10] Esteve, S. J., and Johnson, M. E., "Adaptive Helmholtz Resonators and Passive Vibration Absorbers for Cylinder Interior Noise Control," *Journal of Sound and Vibration*, Vol. 288, No. 4, 2005, pp. 1105–1130. doi:10.1016/j.jsv.2005.01.017

[11] Matsuhisa, H., Ren, B., and Sato, S., "Semi-active Control of Duct Noise by a Volume-Variable Resonator," *Japan Society of Mechanical Engineers International Journal*, Vol. 35, No. 2, 1992, pp. 223–228.

[12] Yamanaka, S., "Application of Helmholtz resonators for Reducing the Combustion Oscillation in a Gas Turbine," International Gas Turbine Congress, Rept. TS-146, Tokyo, Nov. 2003.

[13] Birdsong, C. B., "A Semi-Active Helmholtz Resonator," Ph.D. Dissertation, Department of Mechanical Engineering, Michigan State Univ., East Lansing, MI, Nov. 1999.

[14] Liu, F., Horowitz, S., Nishida, T., Cattafesta, L., and Sheplak, M., "A Tunable Electromechanical Helmholtz Resonator," AIAA Paper 2003-3145, May 2003.

[15] Liu, F., Horowitz, S., Nishida, T., Cattafesta, L., and Shepla, M., "Optimization of an Electromechanical Helmholtz Resonator," AIAA Paper 2006-2524, May 2006.

[16] Horowitz, S., Nishida, T., Cattafesta, L., and Sheplak, M., "Compliant-Backplate Helmholtz Resonators for Active Noise Control Applications," AIAA Paper 2001-0817, Jan. 2001.

[17] Horowitz, S., Nishida, T., Cattafesta, L., and Sheplak, M., "Characterization of Compliant-Backplate Helmholtz Resonators for an Electromechanical Acoustic Liner," AIAA Paper 2002-0666, Jan. 2002.

[18] Zaikin, A. A., and Rudenko, O. V., "A Nonlinear Model of the Helmholtz Resonator with a Movable Wall," *Acoustical Physics*, Vol. 42, No. 3, 1996, pp. 329–333.

[19] Dupere, I. D. J., and Dowling, A. P., "The Absorption of Sound by Helmholtz Resonators with and Without Flow," AIAA Paper 2002-2590, June 2002.

[20] Hersh, A. S., Walker, B. E., and Celano, J. W., "Helmholtz Resonator Impedance Model, Part 1: Nonlinear Behaviour," *AIAA Journal*, Vol. 41, No. 5, 2003, pp. 795–808. doi:10.2514/2.2041

[21] Seybert, A. F., and Ross, D. F., "Experimental Determination of Acoustic Properties Using a Two-Microphone Random-Excitation Technique," *Journal of the Acoustical Society of America*, Vol. 61, No. 5, 1977, pp. 1362–1370. doi:10.1121/1.381403

J. Astley
Associate Editor